RETHINKING LIGHT DECODER-BASED SOLVERS FOR VEHICLE ROUTING PROBLEMS

Anonymous authors
Paper under double-blind review

ABSTRACT

Light decoder-based solvers have gained popularity for solving vehicle routing problems (VRPs) due to their efficiency and ease of integration with reinforcement learning algorithms. However, they often struggle with generalization to larger problem instances or different VRP variants. This paper revisits light decoder-based approaches, analyzing the implications of their reliance on static embeddings and the inherent challenges that arise. Specifically, we demonstrate that in the light decoder paradigm, the encoder is implicitly tasked with capturing information for all potential decision scenarios during solution construction within a single set of embeddings, resulting in high information density. Furthermore, our empirical analysis reveals that the overly simplistic decoder struggles to effectively utilize this dense information, particularly as task complexity increases, which limits generalization to out-of-distribution (OOD) settings. Building on these insights, we show that enhancing the decoder capacity, with a simple addition of identity mapping and a feed-forward layer, can considerably alleviate the generalization issue. Experimentally, our method significantly enhances the OOD generalization of light decoder-based approaches on large-scale instances and complex VRP variants, narrowing the gap with the heavy decoder paradigm.

1   INTRODUCTION

Vehicle Routing Problems (VRPs) are a fundamental class of NP-hard combinatorial optimization problems (COPs) with wide-ranging applications in logistics (Konstantakopoulos et al., 2022), transportation (Garaix et al., 2010), and supply chain management (Dondo et al., 2011). Efficiently solving VRPs is critical for reducing operational costs and enhancing service quality in practice. Traditionally, VRPs have been tackled either using exact solvers (e.g., Gurobi) or heuristic solvers (e.g., LKH-3 (Helsgaun, 2017a)). While these methods can yield high-quality (or even optimal) solutions for small to moderate-sized instances, they often face challenges in scaling to larger problem sizes or adapting to different problem variants without extensive domain expertise or manual tuning.

Neural solvers have emerged as a promising alternative by leveraging advanced deep learning techniques to learn solution strategies directly from data (Bengio et al., 2021). Numerous neural solvers have been proposed for solving VRPs (Bogyrbayeva et al., 2024), with autoregressive construction solvers gaining particular popularity. These solvers sequentially build solutions by adding one feasible node at a time and are valued for their conceptual simplicity and flexibility across different VRP variants. Among them, (heavy encoder) light decoder-based solvers (Vinyals et al., 2015; Kool et al., 2019; Kwon et al., 2020; Kim et al., 2022; Gao et al., 2024; Liu et al., 2024) stand out for their computational efficiency and ease of integration with reinforcement learning (RL) algorithms. These methods typically employ a heavy transformer-based encoder to compute *static* node embeddings [1], followed by a lightweight decoder to construct the solution by sequentially selecting the next node based on these embeddings. While this paradigm has shown promising in-distribution performance, it faces significant challenges in generalizing to out-of-distribution (OOD) instances (Joshi et al., 2021), especially those with larger problem sizes or more complex constraints.

Recent works (Drakulic et al., 2023; Luo et al., 2023) propose a (light encoder) heavy decoder architecture to generate *dynamic* node embeddings, improving generalization on large-scale instances.

---

[1]In this paper, static embedding refers to a set of node embeddings used for all key and value computations in the decoder's attention layers throughout the entire decoding process.

Despite the impressive performance, they exhibit several limitations: 1) their solution construction process is computationally inefficient, as they must re-embed the remaining nodes at each decoding step, resulting in much higher computational costs than light decoder-based solvers; 2) they require a considerable amount of high-quality solutions as labels for supervised training, which may be impractical for less-explored problem variants. Although self-improvement learning (Luo et al., 2024) can help reduce the label burden, advanced search techniques (Pirnay & Grimm, 2024) may still be necessary to generate high-quality pseudo-labels for effective training, introducing an extra layer of complexity to the training process; 3) their versability may be compromised by the policy formulation, as they have to solve problems with an inherently tail-recursive nature. That said, both paradigms have their respective merits, and our goal is to narrow the performance gap between them.

In this paper, we revisit the *light decoder* paradigm by analyzing its inherent limitations, and identifying potential bottlenecks in current methods that hinder their performance. Firstly, we demonstrate that the architecture design of the light decoder paradigm imposes an inherent challenge on the encoder by assigning it an overly complex learning task. As nearly all embedding transformations are performed in a context-agnostic manner by the encoder, it has to encapsulate all relevant information necessary to address any possible future context of solution construction within a single set of static embeddings, resulting in high information density. As the problem size grows, this task becomes exponentially more complex, as the encoder must anticipate and represent an increasingly vast amount of potential sub-problems and decision paths within fixed-size static embeddings. In contrast, the dynamic node embeddings in the heavy decoder paradigm are only responsible for predicting the next step based on the current state, simplifying the decision-making task but sacrificing computational efficiency. Secondly, despite these inherent challenges of the light decoder paradigm, their heavy encoders are still capable of learning valuable static embeddings that effectively address a broad spectrum of sub-problems. However, our empirical analysis reveals that the overly simplistic decoder struggles to effectively leverage the dense information embedded in static embeddings during solution construction and fails to handle tasks with unseen levels of complexity, thereby limiting the model's ability to generalize to OOD problem instances. This suggests that enhancing the decoder's capacity could unlock the latent potential of existing approaches and potentially alleviate the burden on the encoder. Building on these insights into the light and heavy decoder paradigms, we propose a simple yet efficient method that leverages the strengths of each to compensate their respective weaknesses, significantly improving the performance of light decoder-based solvers.

Our contributions are summarized as follows.

- We systematically revisit the light decoder paradigm by thoroughly analyzing its inherent challenges and identifying potential bottlenecks in existing methods, with the goal of enhancing their generalization performance.
- We provide insights into their poor generalization, including the overly complex learning task imposed on the encoder and the inability of the simplistic decoder to effectively leverage the dense information in static embeddings when addressing OOD instances. Based on these insights, we propose ReLD, incorporating simple yet efficient modifications, such as adding identity mapping and a feed-forward layer, to enhance the decoder's capacity.
- We conduct extensive experiments on cross-size and cross-problem benchmarks, and demonstrate the effectiveness of our method in significantly improving both in-distribution and OOD generalization performance of light decoder-based solvers. Notably, our work narrows the performance gap between light and heavy decoder paradigms, reaffirming the potential of light decoder-based solvers when properly adjusted.

2 RETHINKING LIGHT DECODER-BASED SOLVERS

We introduce light decoder-based solvers, where the decoder leverages *static node embeddings as keys and values in its attention layers throughout the entire decoding process*. Hereafter, with a slight abuse of terminology, the terms *static embedding* and *light decoder* will be used interchangeably.

2.1 PRELIMINARIES

VRP. A VRP instance is defined over a graph $G = \{V, E\}$, where $v_i \in V = \{v_i\}_{i=0}^{N}$ represents the node and $e(v_i, v_j) \in E$ represents the edge between node v_i and v_j. A feasible solution τ is
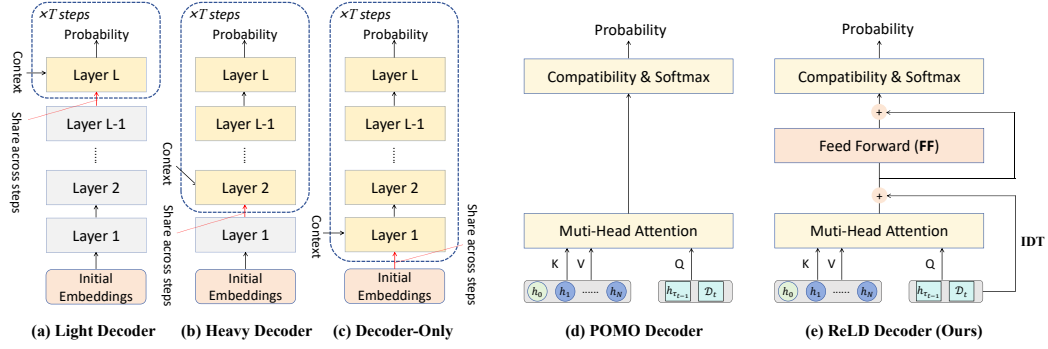
Figure 1: (a)-(c): The primary difference between light decoder, heavy decoder, and decoder-only paradigms lies in the number of prefix layers that are shared across decoding steps. (d)-(e): Decoder structures of POMO and ReLD. QKV in (d) or (e) refers to the query, key and value matrices involve in the computation of MHA as presented in Eq. (4) or (9) (e.g., $Q = h_c$, $K = V = H_t$ in Eq. (4)).

represented as a sequence of nodes that satisfies the problem-specific constraints. For example, a feasible solution in CVRP consists of multiple sub-tours, each of which represents a vehicle starting from the depot node v_0, visiting a subset of customer nodes and returning to the depot node. It is feasible if each customer node is visited exactly once and the total demand in each sub-tour does not exceed the vehicle's capacity limit (i.e., capacity constraint).

Policy Formulation. In theory, the Markov decision process (MDP) of light decoder-based solvers for generating a solution $\tau = (\tau_1, \ldots, \tau_T)$ to a VRP instance should be formulated as follows:

$$p_\theta(\tau|G) = \prod_{t=2}^{T} p_\theta(\tau_t|\tau_1, \tau_{t-1}, s_t, U_t), \tag{1}$$

where p_θ is the policy parameterized by θ, T is the total number of construction steps, τ_t represents the node selected at step t, s_t encapsulates the state variables at step t (e.g., remaining vehicle capacity for CVRP), and U_t denotes the sub-graph of G consisting of only unvisited nodes at step t. It is important to note that at any step t, the policy should be conditioned only on the immediate previous node τ_{t-1} and the initial node τ_1 (i.e., depot node v_0), rather than the entire sequence of previously selected nodes. This reflects the property that the solution to the remaining sub-problem is independent of the sequence of earlier decisions made in VRPs.

Light Decoder-based Architecture. Typically, a transformer-based encoder-decoder architecture is utilized to parameterize the policy p_θ. Given an instance of N customer nodes, each characterized by raw features $x_i \in \mathbb{R}^{d_x}$, the model first projects these features into initial embeddings $h_i^{(0)} \in \mathbb{R}^{d_h}$ through a linear transformation. These initial embeddings are then processed through L encoder layers to generate a final set of static node embeddings $H^{(L)} = (h_0^{(L)}, \ldots, h_N^{(L)})$. Formally, each encoder layer ℓ transforms $H^{(\ell-1)} = \{h_i^{(\ell-1)}\}_{i=0}^{N}$ as follows:

$$\hat{h}_i^{(\ell)} = \text{NORM}\left(h_i^{(\ell-1)} + \text{MHA}(h_i^{(\ell-1)})\right), \tag{2}$$

$$h_i^{(\ell)} = \text{NORM}\left(\hat{h}_i^{(\ell)} + \text{FF}(\hat{h}_i^{(\ell)})\right), \tag{3}$$

where $\text{NORM}(\cdot)$ is a normalization layer, $\text{MHA}(\cdot)$ is a multi-head self-attention layer, and $\text{FF}(\cdot)$ is a feed forward network with ReLU activation. We refer to Kool et al. (2019) for further details. At each decoding step t, the decoder takes as inputs the node embeddings $H_t = \{h_i^{(L)}\}_{i \in F_t}$, with F_t denoting the set of feasible nodes at time t, and a context vector $h_c = [h_{\tau_{t-1}}^{(L)}, \mathcal{D}_t] \in \mathbb{R}^{d_h + d_{attr}}$, with $\mathcal{D}_t \in \mathbb{R}^{d_{attr}}$ denoting dynamic features that capture the state variable s_t in Eq. (1). To aggregate information from node embeddings, the decoder refines the context vector h_c through a multi-head cross-attention layer, using h_c as the query and $H_t \in \mathbb{R}^{|F_t| \times d_h}$ as the key and value, as follows:

$$h_c' = \text{MHA}(h_c, H_t, H_t). \tag{4}$$

3

Finally, with a hyperparameter to clip the logits so as to benefit the policy exploration, the probability p_i of selecting node $i \in F_t$ is calculated as follows:

$$p_i = \text{Softmax}\left(C \cdot \tanh(\frac{(h'_c)^T H_t}{\sqrt{d_h}})\right)_i. \tag{5}$$

Multi-trajectory Strategy. The multi-trajectory strategy has been a default technique for light decoder-based solvers during training and inference since its introduction in Kwon et al. (2020). Specifically, it exploits the symmetries in VRP solution representations by sampling multiple trajectories of an instance, each starting from a different initial node. This approach can be efficiently implemented due to the shared embedding design in light decoder-based solvers, where all trajectories share the same set of static node embeddings, significantly reducing memory consumption. During training, the model parameters θ are optimized to minimize the expected tour length over the training data distribution using the REINFORCE algorithm (Williams, 1992). For each instance, multiple trajectories are generated by varying the starting move, with the baseline value for the policy gradient set to the mean reward (i.e., negative tour length) of all trajectories sampled from that instance. At inference time, multiple trajectories are sampled in parallel, and the one with the minimal cost is selected as the final solution for a given test instance. This strategy effectively enhances exploration of the solution space without incurring significant computational overhead.

2.2 POLICY REFORMULATION

Light decoder-based solvers are characterized by their reliance on *static embeddings*, where the input node representations for computing keys and values in the decoder's attention layers remain unchanged throughout all decoding steps. Most existing approaches reformulate the decoding policy (as in Eq. (1)) in terms of the encoder f_{θ_E} and the decoder g_{θ_D} as follows:

$$p_{\theta_E, \theta_D}(\tau|G) = \prod_{t=2}^{T} g_{\theta_D}(\tau_t|h_{\tau_{t-1}}, s_t, \{h_j\}_{j \in U_t}), \tag{6}$$

where $\{h_i\}_{i=0}^{N} = f_{\theta_E}(G)$ represents the set of node embeddings for the entire graph G computed by the encoder f_{θ_E}. In light decoder-based methods, the decoder g_{θ_D} comprises a shallow network, such as a MHA and single-query attention layer (Kool et al., 2019; Kwon et al., 2020), while the encoder f_{θ_E} is generally a deeper network. In contrast, heavy decoder-based methods feature a deeper decoder paired with a shallow encoder (Luo et al., 2023). Furthermore, designing f_{θ_E} as either an identity mapping or a simple node-wise feed-forward network can approach what are essentially decoder-only solvers (Drakulic et al., 2023).

Gap between Policy Formulations. Unfortunately, there is a gap between the practical policy formulation in Eq. (6) and the principled policy formulation in Eq. (1). Concretely, each node embedding h_j, used for decision-making at each decoding step, inherently contains information about all other (potentially irrelevant) nodes in the graph due to the attention mechanisms in the encoder. Consequently, at each step, the decoder in Eq. (6) is implicitly conditioned on all previously selected nodes, which diverges from the principled policy formulation. This misalignment exhibits the gap between the theory and practical implementations in existing neural solvers. In the following, we explore this discrepancy from an alternative perspective.

Static Embedding as KV Cache. Recent advancements in Large Language Models (LLM) involve using KV Cache techniques to store computed keys and values from previous tokens within attention layers in the decoder, reducing computational time (Shazeer, 2019; Brown, 2020; Ainslie et al., 2023; Touvron et al., 2023). Static embedding in COP shares similar motivation with KV Cache in NLP, aiming to prevent the re-computation of keys and values. However, a fundamental difference exists in the MDP formulation between COP and NLP. In NLP, the process is *generative*: each predicted token is appended to the state (or context) for subsequent predictions, i.e., the context is increasing throughout the decoding process. Caching KV aligns naturally with the generative nature of the task, where each new token depends on the extended historical context, and hence it does not disrupt the original MDP formulation of the task. In contrast, the process in COP is *selective*: the context diminishes as each predicted element (or token) is removed from consideration in subsequent decisions. This reduction in context, contrary to the expansion observed in NLP, implies that *simply reusing KV computed on historical context may introduce irrelevant information to the decision on*

current sub-problem. This increases the learning task's complexity, as the decoder further needs to learn to disentangle irrelevant information from the inputs.

2.3 ANALYSES OF LIGHT DECODER PARADIGM

In the light decoder paradigm, the encoder takes on the complex task of producing context-agnostic node embeddings that are broadly applicable across various sub-problems within the original instance, yielding static embeddings with high information density. Despite the challenging nature of the task, we find that these embeddings are effective in addressing a broad spectrum of sub-problems. Then, the decoder makes decisions based on the current sub-problem at hand to determine the next step. However, our empirical analysis reveals that the simplistic decoder struggles to effectively leverage the dense information in static embeddings and fails to manage tasks with unseen levels of complexity, thereby limiting the model's ability to generalize to OOD problem instances. This highlights the need for a more powerful decoder capable of effectively interpreting and adapting static embeddings to the current context, filtering out irrelevant information and focusing on the features most relevant to the sub-problem at hand. In the following, we delve into each point in detail.

Complex Learning Task for the Encoder. A weak decoder imposes substantial challenges on the encoder's learning task. Since 1) nearly all embedding transformations are performed in a context-agnostic manner by the encoder, and 2) the simplistic decoder lacks the capacity to effectively adjust static embeddings according to the context, the encoder has to encapsulate all relevant information to produce static embeddings that are sufficiently detailed and informative. These static embeddings are expected to handle any potential sub-problem (i.e. context) that may arise during solution construction, resulting in high information density within a single set of embeddings. As the problem size increases, the task becomes exponentially more difficult due to the combinatorial explosion of decision space. Intuitively, this exponential increase in complexity suggests that the optimal strategies for solving problems at different scales may diverge significantly. As the problem size grows, the interactions between nodes become more intricate, and additional constraints or patterns that are not prominent in smaller instances may emerge. Therefore, the strategies learned at smaller scales may not generalize well to larger instances, hindering the model's ability to adapt across various problem sizes. Additionally, since the encoder must allocate its representational capacity across a wide range of possible contexts, the quality of embeddings for individual situations may be diluted. This dilution may diminish the encoder's ability to capture specific features necessary for optimal performance. In contrast, in the heavy decoder paradigm, the model only needs to produce embeddings tailored to predict the next step based on the current sub-problem, which is a much simpler task compared to the encoder's burden in the light decoder paradigm. By decomposing the complex task into predicting one step at a time based on dynamic embeddings, heavy decoder-based solvers avoid the exponentially increasing task complexity associated with larger problem sizes.

Capability of Static Embeddings in Solving Sub-problems. Despite the challenging nature of the encoder task in light decoder-based solvers, we find that the embeddings generated by heavy encoders are effective in addressing a broad spectrum of sub-problems. To empirically support this, we conduct an experiment using node embeddings obtained from CVRP instances to solve randomly sampled sub-instances. For simplicity, instead of generating a large instance and subsampling a set of nodes, we first generate a small instance (i.e., a subproblem) and then add a random set of additional nodes. Note that these two processes are equivalent, as the generation of each node is independent. Specifically, for a uniformly sampled CVRP instance of size n, we introduce an additional set of irrelevant nodes of size $\lceil \delta \times n \rceil$ generated from the same distribution, where δ denotes the extension rate. Then, the encoder processes all $n + \lceil \delta \times n \rceil$ nodes, but only the original n node embeddings are used as inputs to the decoder for decision-making. We conduct experiments on 100 instances and report the average results in Table 1. It can be observed that using embeddings from a larger instance does not significantly affect the performance of light decoder-based solvers, such as POMO (Kwon et al., 2020)). Since the model is unaware of the specific sub-problem it needs to solve in advance, this suggests that static embeddings contain valuable information to solve various sub-problems. Moreover, we conduct similar experiments on heavy decoder-based solvers, such as LEHD (Luo et al., 2023)). In this setup, at each decoding step, we append $\lceil \delta \times n \rceil$ random nodes to the model and filter them out before the final decoder layer, ensuring that the additional nodes pass through the same number of layers as in POMO's encoder. The results reveal that the LEHD model is highly sensitive to the additional context, indicating that most of its layers, unlike those in POMO, are highly specialized for solving a specific sub-problem at each decoding step.

Table 1: Impact of embeddings from an extended graph. Models are trained on CVRP100.

Method	δ	CVRP100 Gap	CVRP200 Gap	CVRP500 Gap
POMO	0.0	1.000%	3.403%	11.135%
	0.5	1.556%	3.968%	10.117%
	1.0	1.880%	4.299%	10.255%
AM	0	7.094%	10.707%	18.145%
	0.5	7.375%	10.729%	20.129%
	1.0	7.642%	11.307%	23.746%
LEHD	0.0	3.648%	3.312%	3.178%
	0.5	11.449%	12.450%	9.999%
	1.0	12.951%	14.456%	12.123%

Table 2: Experiments on fine-tuning and model complexity. Models are trained on CVRP100.

Method	CVRP100 Gap	CVRP200 Gap	CVRP500 Gap	CVRP1000 Gap
POMO	1.000%	3.403%	11.135%	110.632%
Fine-tune Dec	2.620%	4.487%	7.148%	15.202%
Fine-tune Enc	3.061%	4.384%	4.863%	9.627%
Fine-tune All	2.594%	4.132%	5.718%	11.708%
POMON	0.947%	3.864%	13.008%	33.262%
POMON-Enc$^+$	0.890%	2.703%	9.578%	30.198%
POMON-Dec$^+$	0.682%	2.640%	8.185%	18.076%

Inability of Simplistic Decoders. Our empirical results (in Table 2) highlight the inferior generalization performance of light decoder-based solvers on large-scale instances. To further investigate the influence of the encoder and decoder on generalization, we conduct two experiments. First, inspired by the linear probe protocol in self-supervised learning (He et al., 2020; Chen et al., 2020), we fine-tune POMO (pretrained on CVRP100) on large-scale instances. We observe that fine-tuning only the decoder results in relatively poor performance compared to fine-tuning the encoder or performing full fine-tuning. This suggests a potential defect of the decoder architecture, which may complicate the fine-tuning process. Second, we attempt to strengthen the encoder and decoder of POMON (without the normalization layer), respectively. For example, POMON-Enc$^+$ simply incorporates two more layers into the encoder. The results suggest that the decoder may be overly simplistic, as increasing its capability can significantly improve its generalization performance and may reduce the burden on the encoder. This observation is also supported by recent studies (Drakulic et al., 2023; Luo et al., 2023; Zhou et al., 2024b), which show that enhancing the decoder with deeper layers or conditional computation can substantially boost generalization performance. Therefore, we assume the potential bottleneck of light decoder-based solvers lies in their simplistic decoders, which struggle to effectively leverage the dense information in static embeddings and fail to manage tasks with increasing complexity.

3 METHODOLOGY

Building on the insights into the light and heavy decoder paradigms discussed in Section 2, we propose ReLD, which incorporates simple yet efficient modifications to the decoder architecture and training process. ReLD effectively enhances the decoder's capability while preserving the advantages of light decoder-based solvers. The structure of ReLD is illustrated in Fig. 1.

3.1 DIRECT INFLUENCE OF CONTEXT

Existing light decoder-based solvers typically employ a decoder architecture composed of an MHA layer followed by a compatibility layer. The MHA layer aggregates information from the static node embeddings using a context vector h_c to form the query vector h'_c. This query vector is then used by the compatibility layer to compute the probability distribution for the next step, based on the dot-product similarity between h'_c and each node embedding. In this design, h'_c is the only component that captures the context, placing the entire burden of context representation on this single vector. To make the computation of the query vector h'_c clearer, we re-write Eq. (4) as follows:

$$h'_c = \text{MHA}(h_c, H_t, H_t) = \sum_{s=1}^{S} W_s^O \sum_{i \in F_t} u_{s,i} W_s^V h_i = \sum_{s=1}^{S} \sum_{i \in F_t} u_{s,i} v_{s,i}, \quad (7)$$

$$\text{where } u_{s,i} = \text{Softmax}\left(\frac{(W_s^Q h_c)^T W_s^K H_t}{\sqrt{d_h}}\right)_i, \quad v_{s,i} = W_s^O W_s^V h_i. \quad (8)$$

Here, S is the number of attention heads, $W_s^O, W_s^Q, W_s^K, W_s^V$ are the projection matrices in the s-th attention head, and $H_t = \{h_i\}_{i \in F_t}$ denotes the static node embeddings. We omit the superscript (L) for simplicity of notation. This design implies that the influence of the context h_c on h'_c is only mediated through the attention weights $u_{s,i}$, without directly modifying the combined vectors.

Such an indirect incorporation of context may lead to inefficient utilization of context information, especially in tasks with complex constraints where dynamic context is crucial for decision-making.

To address this limitation, we propose directly integrating context information into the embedding space, rather than relying solely on the attention weights. Specifically, we suggest adding an residual connection (He et al., 2016) between the context vector h_c and the query vector h'_c, thereby embedding context-aware information directly into the representation:

$$h'_c = \text{MHA}(h_c, H_t, H_t) + \text{IDT}(h_c). \tag{9}$$

In practice, $h_c = [h_{\tau_{t-1}}, \mathcal{D}_t]$ typically has a different shape compared to h'_c, so the identity mapping function $\text{IDT}(\cdot)$ must reshape the original input. To effectively preserve the information of the last node location h_{last} while maintaining simplicity, we define the function $\text{IDT}(\cdot)$ as follows:

$$\text{IDT}(h_c) = h_{\tau_{t-1}} + W^{\text{IDT}} \mathcal{D}_t, \tag{10}$$

where W^{IDT} is a learnable parameter that projects $\mathcal{D}_t$ to the same dimension as $h_{\tau_{t-1}}$.

3.2 POWERFUL QUERY

A key component of the decoder is the context-aware query vector h'_c, which is used to compute attention scores over the node embeddings and ultimately determine the probability distribution over the next possible nodes. This query vector is crucial, as it is the only element in the computation that incorporates the current context of the decision-making. In existing implementations, as shown in Eq. (7), h'_c is computed as a weighted combination of the node embeddings. The computation follows a largely linear form with respect to the fixed sets of value vectors $v_{s,i}$, with the only non-linearity introduced through the attention weights $u_{s,i}$. This inherent linearity may limit the decoder's capacity to model complex relationships and adapt the embeddings based on the context.

Considering the importance of non-linearity in enabling neural networks to model complex functions (Cybenko, 1989), we propose to enhance the decoder's representation capacity by introducing non-linearity into the computation of h'_c. Intuitively, to more effectively transform the context information, non-linearity should be introduced after the context has been fully aggregated. This suggests that adding non-linearity after the MHA layer, where the global context is integrated, would have a bigger impact. Drawing inspiration from the observation that the overall architecture of transformer blocks, rather than solely the self-attention mechanism, plays a significant role in the model's performance (Raghu et al., 2021; Yu et al., 2022), we propose incorporating a feed-forward network with residual connections into the decoder as follows:

$$q_c = h'_c + \text{FF}(h'_c) = h'_c + \sigma(W_2 \sigma(W_1 h'_c + b_1) + b_2), \tag{11}$$

where W_1, W_2, b_1, and b_2 are the parameters of the feed-forward layer, and σ denotes the ReLU activation function. This modification, along with the one presented in Eq. (9), transforms the decoder into a transformer block with a single query, adding non-linear processing capabilities to the query vector computation. In doing so, it provides the encoder with greater flexibility in designing the embedding space and potentially alleviates the burden imposed on it. Note that our modification is computationally efficient, as the additional step-wise running time is independent of the number of nodes, and therefore does not affect the overall asymptotic time complexity of the decoder. This makes it a practical and effective enhancement for light decoder-based methods.

3.3 GENERALIZABLE TRAINING

Distance Heuristic. Recent advancements have incorporated distance heuristics into the learned policy (Jin et al., 2023; Gao et al., 2024; Wang et al., 2024; Zhou et al., 2024a) to enhance generalization on larger-scale instances. Building on this idea, we add a negative logarithmic distance heuristic score to the output of the compatibility layer in the decoder, modifying Eq. (5) into:

$$p_i = \text{Softmax}\left(C \cdot \tanh(\frac{(q_c)^T H_t}{\sqrt{d_h}} - \log(dist_i))\right)_i, \tag{12}$$

where $dist_i$ denotes the distance between node i and the last selected node τ_{t-1}.

Varying Attribute. Recent work have also introduced several strategies to improve the generalization on large-scale instances, such as training on varying instance sizes (Drakulic et al., 2023; Zhou et al., 2023; Luo et al., 2023; Wang et al., 2024; Zhou et al., 2024a) and vehicle capacities (Gao et al., 2024). We also adopt these strategies in our approach (see Section 4.1).

Table 3: Results on synthetic CVRP instances.

Method	CVRP100		CVRP200		CVRP500		CVRP1000	
	Gap	Time	Gap	Time	Gap	Time	Gap	Time
LKH3	*	12 h	*	2.1 h	*	5.5 h	*	7.1h
HGS	-0.533%	4.5 h	-1.126%	1.4 h	-1.794%	4 h	-2.162%	5.3 h
GLOP-G (LKH3)*	-	-	-	-	-	-	6.903%	1.7m
BQ greedy*	2.726%	1.3 m	2.972%	10 s	3.248%	0.69m	5.892%	1.59m
LEHD greedy	3.648%	0.38m	3.312%	2 s	3.178%	15s	**4.912%**	1.34m
MDAM bs50*	2.211%	25m	4.304%	3m	10.498%	12m	27.814%	47m
POMO augx8	1.004%	1.07m	3.403%	2s	11.135%	13s	110.632%	0.88m
ELG augx8	1.207%	3.18 m	2.553%	7s	5.472%	0.44m	10.760%	1.42m
ReLD augx8	**0.960%**	1.34m	**1.654%**	2s	**2.975%**	15s	6.757%	0.91m

Table 4: Results on CVRPLib Set-X instances.

	$N \leq 200$ (22 instances)	$200 < N \leq 500$ (46 instances)	$500 < N \leq 1000$ (32 instances)	Total (100 instances)
BKS	*	*	*	*
LEHD greedy*	11.35%	9.45%	17.74%	12.52%
BQ greedy*	-	-	-	9.94%
INViT-3V*	6.52%	9.11%	10.21%	-
POMO	5.63%	9.25%	18.85%	11.52%
ICAM no-aug*	5.14%	4.44%	5.17%	4.83%
ELG no-aug	6.25%	7.58%	10.02%	8.07%
ELG	4.51%	5.52%	7.81%	6.03%
MTL	9.49%	10.96%	16.80%	12.51%
MVMoE	4.74%	9.97%	19.60%	11.90%
ReLD-MTL	3.31%	5.84%	9.05%	6.31%
ReLD-MoEL	3.14%	5.75%	8.83%	6.16%
ReLD-MoEL$^+$	**2.41%**	**3.40%**	**4.52%**	**3.54%**
ReLD no-aug	3.36%	3.93%	5.12%	4.18%
ReLD	2.53%	3.44%	4.64%	3.62%

4 EXPERIMENTAL RESULTS AND ANALYSIS

In this section, we present empirical results from experiments on synthetic CVRP instances of various scales, multi-task cross-problem learning across 16 VRP variants, and the CVRPLib benchmark datasets to demonstrate the effectiveness of the proposed ReLD method. All experiments were conducted using a single Nvidia A800 GPU with 80GB of memory.

Baselines. 1) *Traditional Solvers*: We utilize SOTA non-learning solvers LKH3 (Helsgaun, 2017b) and HGS (Vidal, 2022), which are known for providing strong results on VRPs. In line with previous work (Luo et al., 2023), the performance gaps are computed relative to LKH3, even though HGS generally produces slightly better results. 2) *Learning-based Solvers*: We retrain the POMO model (Kwon et al., 2020) for 5,000 epochs, with 10,000 instances per epoch and batch size of 64. Additionally, we utilize the publicly released available models MDAM (Xin et al., 2021a), BQ (Drakulic et al., 2023), ELG (Gao et al., 2024), LEHD (Luo et al., 2023), and GLOP (Ye et al., 2024). Results for INViT (Fang et al., 2024) and ICAM (Zhou et al., 2024a) are obtained from their original papers.

4.1 CROSS-SIZE

Problem Setting. We first evaluate performance on the CVRP using the test dataset introduced in (Luo et al., 2023), which consists of 10,000 instances with 100 nodes, and 128 instances for each problem size of 200, 500, and 1,000 nodes. The corresponding vehicle capacity settings for these problem scales are 50, 80, 100, and 250, respectively.

Model Setting. Based on POMO (Kwon et al., 2020), we remove normalization layers in the encoder and add identity mapping (Section 3.1), feed forward layer (Section 3.2) and distance score (Section 3.3) to decoder to obtain ReLD.

Training Setting. ReLD employs the same training algorithm as POMO (Kwon et al., 2020), but is trained over 90 epochs, with each epoch comprising 600,000 training instances and a batch size of 120. We use the Adam optimizer with an initial learning rate of 1e-4, which is decayed by a factor of 0.1 at the 70th and 80th epochs. Weight decay is set to zero. For generating the training data, we first sample a problem size from a discrete uniform distribution, Uniform(40, 100). Following the standard data generation procedure outlined in (Kool et al., 2019), node coordinates and demands are generated uniformly. To ensure adaptability to varying attribute (Section 3.3), we randomly sample an expected route size r (average number of nodes in a route) from a triangular distribution $T(3, 6, 25)$ (Uchoa et al., 2017) for each instance, the vehicle capacity of which is set to $\lceil r\bar{D} \rceil$, where $\bar{D}$ represents the mean demand of the nodes in the instance. It takes 39 hours with 18131MiB GPU memory to train ReLD.

Inference Setting. For all neural solvers, we adopt the greedy rollout strategy. To ensure comparable runtime across baselines, we set the number of rollout trajectories K for all light decoder-based methods (POMO, ELG, ReLD) to $min(100, N)$, where N represents the problem size. To initialize each trajectory, we input all the nodes with full capacity to the decoder and select top K moves with respect to the output probability distribution.

Results. The results on uniformly generated CVRP instances are presented in Table 3 (the superscript asterisk (*) on method denotes that the results of the method are directly obtained from the original paper). ReLD consistently outperforms other learning-based solvers at all scales except

Table 5: Performance on 1K test instances of 16 VRP variants.

Method	CVRP Obj.	Gap	Time	VRPTW Obj.	Gap	Time	OVRP Obj.	Gap	Time	VRPL Obj.	Gap	Time
HGS	15.504	*	9.1m	24.339	*	19.6m	-	-	-	-	-	-
LKH3	15.590	0.556%	18.0m	24.721	1.584%	7.8m	10.010	*	5.3m	16.496	*	16.0m
OR-Tools	15.935	2.751%	3.5h	25.212	3.482%	3.5h	9.842	0.122%	3.5h	16.004	1.444%	3.5h
POMO	15.734	1.488%	9s	25.367	4.307%	11s	10.044	2.192%	8s	15.785	0.093%	9s
POMO-MTL	15.790	1.846%	9s	25.610	5.313%	11s	10.169	3.458%	8s	15.846	0.479%	9s
MVMoE-L	15.771	1.728%	10s	25.519	4.927%	11s	10.145	3.214%	9s	15.821	0.323%	10s
MVMoE	15.760	1.653%	11s	25.512	4.903%	12s	10.138	3.136%	10s	15.812	0.261%	11s
ReLD-MTL	15.723	1.416%	10s	25.432	4.561%	11s	10.057	2.321%	9s	15.773	0.020%	10s
ReLD-MoEL	15.713	**1.354%**	10s	25.403	4.444%	11s	10.050	2.260%	9s	**15.768**	**-0.016%**	10s
ReLD-MoEL$^+$	15.739	1.515%	10s	25.445	4.621%	11s	10.084	2.592%	9s	15.788	0.113%	10s

Method	VRPB Obj.	Gap	Time	OVRPTW Obj.	Gap	Time	OVRPB Obj.	Gap	Time	OVRPL Obj.	Gap	Time
OR-Tools	11.878	*	3.5h	14.380	*	3.5h	8.365	*	3.5h	9.790	*	3.5h
POMO	11.993	0.995%	9s	**14.728**	**2.467%**	11s	-	-	-	-	-	-
POMO-MTL	12.072	1.674%	9s	15.008	4.411%	11s	8.979	7.335%	8s	10.126	3.441%	9s
MVMoE-L	12.036	1.368%	10s	14.940	3.941%	11s	8.972	7.243%	9s	10.106	3.244%	10s
MVMoE	12.027	1.285%	11s	14.927	3.852%	12s	8.959	7.088%	10s	10.097	3.148%	11s
ReLD-MTL	11.981	0.901%	10s	14.818	3.103%	11s	8.814	5.361%	9s	10.014	2.310%	10s
ReLD-MoEL	**11.969**	**0.801%**	10s	14.804	3.000%	11s	8.804	5.239%	9s	**10.007**	**2.233%**	10s
ReLD-MoEL$^+$	11.981	0.887%	10s	14.848	3.304%	11s	**8.794**	**5.113%**	9s	10.040	2.567%	10s

Method	VRPBL Obj.	Gap	Time	VRPBTW Obj.	Gap	Time	VRPLTW Obj.	Gap	Time	OVRPBL Obj.	Gap	Time
OR-Tools	11.790	*	3.5h	25.496	*	3.5h	25.195	*	3.5h	8.348	*	3.5h
POMO-MTL	11.998	1.793%	9s	27.319	7.413%	11s	25.619	1.920%	8s	8.961	7.343%	9s
MVMoE-L	11.960	1.473%	10s	27.265	7.190%	11s	25.529	1.545%	9s	8.957	7.300%	10s
MVMoE	11.945	1.346%	11s	27.236	7.078%	12s	25.514	1.471%	10s	8.942	7.115%	11s
ReLD-MTL	11.905	1.005%	10s	27.144	6.735%	11s	25.433	1.167%	9s	8.800	5.411%	10s
ReLD-MoEL	**11.894**	**0.917%**	10s	**27.106**	**6.574%**	11s	**25.415**	**1.089%**	9s	8.786	5.247%	10s
ReLD-MoEL$^+$	11.908	1.024%	10s	27.166	6.806%	11s	25.456	1.258%	9s	**8.779**	**5.154%**	10s

Method	OVRPBTW Obj.	Gap	Time	OVRPLTW Obj.	Gap	Time	VRPBLTW Obj.	Gap	Time	OVRPBLTW Obj.	Gap	Time
OR-Tools	14.384	*	3.5h	14.279	*	3.5h	25.342	*	3.5h	14.250	*	3.5h
POMO-MTL	15.879	10.453%	9s	14.896	4.374%	11s	27.247	7.746%	8s	15.738	10.498%	9s
MVMoE-L	15.841	10.188%	10s	14.839	3.971%	11s	27.177	7.473%	9s	15.706	10.263%	10s
MVMoE	15.808	9.948%	11s	14.828	3.903%	12s	27.142	7.332%	10s	15.671	10.009%	11s
ReLD-MTL	15.711	9.288%	10s	14.721	3.159%	11s	**27.042**	6.937%	9s	15.555	9.215%	10s
ReLD-MoEL	15.697	**9.184%**	10s	**14.707**	**3.054%**	11s	27.044	**6.915%**	9s	**15.550**	**9.171%**	10s
ReLD-MoEL$^+$	15.728	9.403%	10s	14.744	3.318%	11s	27.078	7.106%	9s	15.599	9.516%	10s

for CVRP1000, while achieving similar or lower computational time. For CVRP1000, ReLD remains highly competitive, surpassing most neural solvers. However, solvers like BQ and LEHD still demonstrate superior performance at this scale, indicating that a performance gap persists between light decoder-based methods and heavy decoder or decoder-only architectures for larger instances. This finding suggests the need to further enhance the decoder's capacity in light decoder-based models to close this gap.

4.2 CROSS-PROBLEM

We follow all the problem setting, training setting, and evaluation setting used in Zhou et al. (2024b).

Model Setting. We remove all the normalization layers in the encoder and add identity mapping (Section 3.1), feed forward layer (Section 3.2) to the original POMO-MTL and MVMoE-light to obtain the ReLD-MTL and ReLD-MoEL. Notably, original MVMoE-light utilizes an MoE layer to replace the linear layer in the decoder to transform the results obtained from multiple attention heads. For simplicity and fair comparison, we use the original POMO decoder architecture with added identity mapping and feed forward layer in both of the ReLD-MTL and ReLD-MoEL. We also employ the training techniques in Section 3.3 on ReLD-MoEL, denoted as ReLD-MoEL$^+$.

Results. The results on all the VRP variants are shown in Table 5 and Table 7 (see Appendix). It is quite clear that all the ReLD models outperform the POMO-MTL, MVMoE-L and MVMoE baselines on all the studied VRP variants by a significant margin. **Notably**, both the ReLD-MTL and ReLD-MoEL outperform the single-task POMO that is specifically trained on the CVRP, VRPL and VRPB. An even more surprising result is that ReLD-MoEL surpasses the strong LKH3 traditional solver on VRPL, achieving a negative gap. The improvement becomes even more pronounced in the generalization to unseen VRP variants (the last 10 variaints in Table 5), with an average gap improvement of 1.1% and 1.0% for ReLD-MTL and ReLD-MoEL, respectively, compared to their original counterparts. This demonstrates the superior ability of ReLD to handle varying constraints effectively. On the other hand, ReLD-MoEL$^+$ underperforms relative to other ReLD models on most problems, though it still significantly outperforms all baselines. This suggests that the tech-

niques employed in Section 3.3 may trade off in-distribution performance to gain stronger out-of-distribution generalization, aligning with the observations in Section 4.4.

4.3 BENCHMARK PERFORMANCE

We also evaluate our ReLD on the well known benchmark dataset CVRPLib Set-X (Uchoa et al., 2017) and Set-XXL. Specifically, we divide CVRPLib Set-X (Uchoa et al., 2017) into 3 subsets according to the scale the of instances, each with range $N \leq 200$, $200 < N \leq 500$ and $500 < N \leq 1000$. For Set-XXL, we select instances with size $3000 \leq N \leq 16000.$

Inference. On both datasets, light decoder-based models run with a maximum of 100 trajectory and augmentation x8 (Kwon et al., 2020) is used by default.

Results. The results on Set-X and Set-XXL are presented in Table 4 and Table 8 (see Appendix), respectively. Interestingly, heavy decoder methods like LEHD show inferior performance on Set-X instances, especially when compared to the lighter decoder-based methods. ReLD models, including both ReLD-MTL and ReLD-MoEL, consistently outperform the baseline methods without distance heuristic across all instance sizes. For the models that involve using advanced techniques like distance heuristic, ReLD-MoEL$^+$ achieves the best results. Such surprising results suggest that it is a generalizable foundational model. Furthermore, ReLD demonstrates a significant margin of improvement over all baseline methods on the four large scale real-world instances from Set-XXL, further validating the generalizability of the proposed methods.

4.4 ABLATION STUDY

We conduct ablation study to gain insights for the contribution of each components in ReLD for the overall performance. Main ablation results are presented in Table 10 (see Appendix).

Identity Mapping is Crucial for OOD Size Generalization. The introduction of identity mapping significantly improves generalization to larger problem sizes for both POMO and POMON (POMO without the normalization layer), highlighting its critical role in handling out-of-distribution (OOD) instances. Additionally, it provides minor improvements for smaller problem sizes, indicating that it enhances generalization without sacrificing in-distribution performance.

Feed Forward Layer is Crucial for In-Distribution Learning. Adding feed-forward layer to POMON reduces the gap on CVRP100 from 0.95% to 0.66% (POMON v.s. POMON+FF), a significant improvement in in-distribution learning. However, this modification is less effective for larger scales without the identity mapping, as seen on CVRP1000.

ReLD Improves Generalization Performance to Larger Size. Adding the feed-forward layer alongside identity mapping combines their strengths, resulting in significant improvements in both in-distribution learning and OOD size generalization (POMON vs. POMON+IDT+FF). Additionally, incorporating the distance heuristic and training with varying attributes further boosts generalization, though with a slight trade-off in in-distribution performance. The combination of identity mapping and the feed-forward layer provides a comprehensive improvement across all problem scales, effectively reducing the performance gap as problem size increases and demonstrating the effectiveness of the proposed architectural enhancements in various settings.

5 CONCLUSION

This paper systematically revisits the light decoder paradigm, analyzes its inherent challenges, compares it with the heavy decoder paradigm, and identifies potential bottlenecks in existing methods. We offer valuable insights and propose ReLD, a simple yet effective approach to narrow the gap between these two paradigms. Extensive experiments on cross-size and cross-problem benchmarks demonstrate the effectiveness of our method. One limitation is that the proposed method still lags behind heavy decoder-based solvers and faces challenges with very large-scale instances, which may require advanced techniques such as linear attention. We leave the development of more efficient and powerful light decoder-based solvers for future work.

REFERENCES

Joshua Ainslie, James Lee-Thorp, Michiel de Jong, Yury Zemlyanskiy, Federico Lebrón, and Sumit Sanghai. Gqa: Training generalized multi-query transformer models from multi-head checkpoints. *arXiv preprint arXiv:2305.13245*, 2023.

Uri Alon and Eran Yahav. On the bottleneck of graph neural networks and its practical implications. *arXiv preprint arXiv:2006.05205*, 2020.

Thomas Bachlechner, Bodhisattwa Prasad Majumder, Henry Mao, Gary Cottrell, and Julian McAuley. Rezero is all you need: Fast convergence at large depth. In *Uncertainty in Artificial Intelligence*, pp. 1352–1361. PMLR, 2021.

Irwan Bello, Hieu Pham, Quoc V. Le, Mohammad Norouzi, and Samy Bengio. Neural combinatorial optimization with reinforcement learning. In *International Conference on Learning Representations Workshop Track*, 2017.

Yoshua Bengio, Andrea Lodi, and Antoine Prouvost. Machine learning for combinatorial optimization: a methodological tour d'horizon. *European Journal of Operational Research*, 290(2): 405–421, 2021.

Federico Berto, Chuanbo Hua, Junyoung Park, Laurin Luttmann, Yining Ma, Fanchen Bu, Jiarui Wang, Haoran Ye, Minsu Kim, Sanghyeok Choi, Nayeli Gast Zepeda, André Hottung, Jianan Zhou, Jieyi Bi, Yu Hu, Fei Liu, Hyeonah Kim, Jiwoo Son, Haeyeon Kim, Davide Angioni, Wouter Kool, Zhiguang Cao, Jie Zhang, Kijung Shin, Cathy Wu, Sungsoo Ahn, Guojie Song, Changhyun Kwon, Lin Xie, and Jinkyoo Park. Rl4co: an extensive reinforcement learning for combinatorial optimization benchmark. *arXiv preprint arXiv:2306.17100*, 2024.

Jieyi Bi, Yining Ma, Jiahai Wang, Zhiguang Cao, Jinbiao Chen, Yuan Sun, and Yeow Meng Chee. Learning generalizable models for vehicle routing problems via knowledge distillation. In *Advances in Neural Information Processing Systems*, volume 35, pp. 31226–31238, 2022.

Aigerim Bogyrbayeva, Meraryslan Meraliyev, Taukekhan Mustakhov, and Bissenbay Dauletbayev. Machine learning to solve vehicle routing problems: A survey. *IEEE Transactions on Intelligent Transportation Systems*, 2024.

Tom B Brown. Language models are few-shot learners. *arXiv preprint arXiv:2005.14165*, 2020.

Ting Chen, Simon Kornblith, Mohammad Norouzi, and Geoffrey Hinton. A simple framework for contrastive learning of visual representations. In *International conference on machine learning*, pp. 1597–1607. PMLR, 2020.

Xinyun Chen and Yuandong Tian. Learning to perform local rewriting for combinatorial optimization. In *Advances in Neural Information Processing Systems*, volume 32, pp. 6281–6292, 2019.

Paulo da Costa, Jason Rhuggenaath, Yingqian Zhang, and Alp Eren Akçay. Learning 2-opt heuristics for the traveling salesman problem via deep reinforcement learning. In *Asian Conference on Machine Learning*, pp. 465–480, 2020.

George Cybenko. Approximation by superpositions of a sigmoidal function. *Mathematics of control, signals and systems*, 2(4):303–314, 1989.

Rodolfo Dondo, Carlos A Méndez, and Jaime Cerdá. The multi-echelon vehicle routing problem with cross docking in supply chain management. *Computers & Chemical Engineering*, 35(12): 3002–3024, 2011.

Darko Drakulic, Sofia Michel, Florian Mai, Arnaud Sors, and Jean-Marc Andreoli. Bq-nco: Bisimulation quotienting for efficient neural combinatorial optimization. In *Advances in Neural Information Processing Systems*, volume 36, 2023.

Han Fang, Zhihao Song, Paul Weng, and Yutong Ban. Invit: A generalizable routing problem solver with invariant nested view transformer. *arXiv preprint arXiv:2402.02317*, 2024.

Zhang-Hua Fu, Kai-Bin Qiu, and Hongyuan Zha. Generalize a small pre-trained model to arbitrarily large tsp instances. In *Proceedings of the AAAI Conference on Artificial Intelligence*, volume 35, pp. 7474–7482, 2021.

Chengrui Gao, Haopu Shang, Ke Xue, Dong Li, and Chao Qian. Towards generalizable neural solvers for vehicle routing problems via ensemble with transferrable local policy. In *IJCAI*, 2024.

Thierry Garaix, Christian Artigues, Dominique Feillet, and Didier Josselin. Vehicle routing problems with alternative paths: An application to on-demand transportation. *European Journal of Operational Research*, 204(1):62–75, 2010.

Simon Geisler, Johanna Sommer, Jan Schuchardt, Aleksandar Bojchevski, and Stephan Günnemann. Generalization of neural combinatorial solvers through the lens of adversarial robustness. In *International Conference on Learning Representations*, 2022.

Nathan Grinsztajn, Daniel Furelos-Blanco, Shikha Surana, Clément Bonnet, and Thomas D Barrett. Winner takes it all: Training performant RL populations for combinatorial optimization. In *Advances in Neural Information Processing Systems*, 2023.

Kaiming He, Xiangyu Zhang, Shaoqing Ren, and Jian Sun. Deep residual learning for image recognition. In *Proceedings of the IEEE conference on computer vision and pattern recognition*, pp. 770–778, 2016.

Kaiming He, Haoqi Fan, Yuxin Wu, Saining Xie, and Ross Girshick. Momentum contrast for unsupervised visual representation learning. In *Proceedings of the IEEE/CVF conference on computer vision and pattern recognition*, pp. 9729–9738, 2020.

Keld Helsgaun. An extension of the lin-kernighan-helsgaun tsp solver for constrained traveling salesman and vehicle routing problems. *Roskilde: Roskilde University*, pp. 24–50, 2017a.

Keld Helsgaun. *An Extension of the Lin-Kernighan-Helsgaun TSP Solver for Constrained Traveling Salesman and Vehicle Routing Problems: Technical report*. Roskilde Universitet, December 2017b.

André Hottung, Mridul Mahajan, and Kevin Tierney. PolyNet: Learning diverse solution strategies for neural combinatorial optimization. *arXiv preprint arXiv:2402.14048*, 2024.

Qingchun Hou, Jingwei Yang, Yiqiang Su, Xiaoqing Wang, and Yuming Deng. Generalize learned heuristics to solve large-scale vehicle routing problems in real-time. In *International Conference on Learning Representations*, 2023.

Yan Jin, Yuandong Ding, Xuanhao Pan, Kun He, Li Zhao, Tao Qin, Lei Song, and Jiang Bian. Pointerformer: Deep reinforced multi-pointer transformer for the traveling salesman problem. In *Proceedings of the AAAI Conference on Artificial Intelligence*, volume 37, pp. 8132–8140, 2023.

Chaitanya K Joshi, Thomas Laurent, and Xavier Bresson. An efficient graph convolutional network technique for the travelling salesman problem. *arXiv preprint arXiv:1906.01227*, 2019.

Chaitanya K Joshi, Quentin Cappart, Louis-Martin Rousseau, and Thomas Laurent. Learning tsp requires rethinking generalization. In *International Conference on Principles and Practice of Constraint Programming*, 2021.

Minsu Kim, Junyoung Park, and Jinkyoo Park. Sym-nco: Leveraging symmetricity for neural combinatorial optimization. In *Advances in Neural Information Processing Systems*, volume 35, pp. 1936–1949, 2022.

Minsu Kim, Sanghyeok Choi, Jiwoo Son, Hyeonah Kim, Jinkyoo Park, and Yoshua Bengio. Ant colony sampling with gflownets for combinatorial optimization. *arXiv preprint arXiv:2403.07041*, 2024.

Grigorios D Konstantakopoulos, Sotiris P Gayialis, and Evripidis P Kechagias. Vehicle routing problem and related algorithms for logistics distribution: A literature review and classification. *Operational research*, pp. 1–30, 2022.

Wouter Kool, Herke van Hoof, and Max Welling. Attention, learn to solve routing problems! In *International Conference on Learning Representations*, 2019.

Yeong-Dae Kwon, Jinho Choo, Byoungjip Kim, Iljoo Yoon, Youngjune Gwon, and Seungjai Min. Pomo: Policy optimization with multiple optima for reinforcement learning. In *Advances in Neural Information Processing Systems*, volume 33, pp. 21188–21198, 2020.

Yeong-Dae Kwon, Jinho Choo, Iljoo Yoon, Minah Park, Duwon Park, and Youngjune Gwon. Matrix encoding networks for neural combinatorial optimization. In *Advances in Neural Information Processing Systems*, volume 34, 2021.

Sirui Li, Zhongxia Yan, and Cathy Wu. Learning to delegate for large-scale vehicle routing. In *Advances in Neural Information Processing Systems*, volume 34, pp. 26198–26211, 2021.

Fei Liu, Xi Lin, Zhenkun Wang, Qingfu Zhang, Tong Xialiang, and Mingxuan Yuan. Multi-task learning for routing problem with cross-problem zero-shot generalization. In *Proceedings of the 30th ACM SIGKDD Conference on Knowledge Discovery and Data Mining*, pp. 1898–1908, 2024.

Hao Lu, Xingwen Zhang, and Shuang Yang. A learning-based iterative method for solving vehicle routing problems. In *International Conference on Learning Representations*, 2020.

Fu Luo, Xi Lin, Fei Liu, Qingfu Zhang, and Zhenkun Wang. Neural combinatorial optimization with heavy decoder: Toward large scale generalization. In *Advances in Neural Information Processing Systems*, volume 36, pp. 8845–8864, 2023.

Fu Luo, Xi Lin, Zhenkun Wang, Tong Xialiang, Mingxuan Yuan, and Qingfu Zhang. Self-improved learning for scalable neural combinatorial optimization. *arXiv preprint arXiv:2403.19561*, 2024.

Yining Ma, Jingwen Li, Zhiguang Cao, Wen Song, Le Zhang, Zhenghua Chen, and Jing Tang. Learning to iteratively solve routing problems with dual-aspect collaborative transformer. In *Advances in Neural Information Processing Systems*, volume 34, pp. 11096–11107, 2021.

Yining Ma, Zhiguang Cao, and Yeow Meng Chee. Learning to search feasible and infeasible regions of routing problems with flexible neural k-opt. In *Advances in Neural Information Processing Systems*, 2023.

Yimeng Min, Yiwei Bai, and Carla P Gomes. Unsupervised learning for solving the travelling salesman problem. In *Advances in Neural Information Processing Systems*, 2023.

Mohammadreza Nazari, Afshin Oroojlooy, Martin Takáč, and Lawrence V Snyder. Reinforcement learning for solving the vehicle routing problem. In *Advances in Neural Information Processing Systems*, pp. 9861–9871, 2018.

Jonathan Pirnay and Dominik G. Grimm. Self-improvement for neural combinatorial optimization: Sample without replacement, but improvement. *Transactions on Machine Learning Research*, 2024. ISSN 2835-8856. URL https://openreview.net/forum?id=agT8ojoH0X. Featured Certification.

Ruizhong Qiu, Zhiqing Sun, and Yiming Yang. Dimes: A differentiable meta solver for combinatorial optimization problems. In *Advances in Neural Information Processing Systems*, volume 35, pp. 25531–25546, 2022.

Maithra Raghu, Thomas Unterthiner, Simon Kornblith, Chiyuan Zhang, and Alexey Dosovitskiy. Do vision transformers see like convolutional neural networks? *Advances in neural information processing systems*, 34:12116–12128, 2021.

Noam Shazeer. Fast transformer decoding: One write-head is all you need. *arXiv preprint arXiv:1911.02150*, 2019.

Zhiqing Sun and Yiming Yang. Difusco: Graph-based diffusion solvers for combinatorial optimization. In *NeurIPS*, volume 36, pp. 3706–3731, 2023.

Hugo Touvron, Louis Martin, Kevin Stone, Peter Albert, Amjad Almahairi, Yasmine Babaei, Nikolay Bashlykov, Soumya Batra, Prajjwal Bhargava, Shruti Bhosale, et al. Llama 2: Open foundation and fine-tuned chat models. *arXiv preprint arXiv:2307.09288*, 2023.

Eduardo Uchoa, Diego Pecin, Artur Pessoa, Marcus Poggi, Thibaut Vidal, and Anand Subramanian. New benchmark instances for the capacitated vehicle routing problem. *European Journal of Operational Research*, 257(3):845–858, 2017.

Thibaut Vidal. Hybrid genetic search for the cvrp: Open-source implementation and swap* neighborhood. *Computers & Operations Research*, 140:105643, 2022.

Oriol Vinyals, Meire Fortunato, and Navdeep Jaitly. Pointer networks. In *Advances in neural information processing systems*, volume 28, 2015.

Yang Wang, Ya-Hui Jia, Wei-Neng Chen, and Yi Mei. Distance-aware attention reshaping: Enhance generalization of neural solver for large-scale vehicle routing problems. *arXiv preprint arXiv:2401.06979*, 2024.

Ronald J Williams. Simple statistical gradient-following algorithms for connectionist reinforcement learning. *Machine learning*, 8:229–256, 1992.

Yaoxin Wu, Wen Song, Zhiguang Cao, Jie Zhang, and Andrew Lim. Learning improvement heuristics for solving routing problems. *IEEE Transactions on Neural Networks and Learning Systems*, 33(9):5057–5069, 2021.

Yifan Xia, Xianliang Yang, Zichuan Liu, Zhihao Liu, Lei Song, and Jiang Bian. Position: Rethinking post-hoc search-based neural approaches for solving large-scale traveling salesman problems. In *International Conference on Machine Learning*, 2024.

Liang Xin, Wen Song, Zhiguang Cao, and Jie Zhang. Multi-decoder attention model with embedding glimpse for solving vehicle routing problems. In *Proceedings of the AAAI Conference on Artificial Intelligence*, volume 35, pp. 12042–12049, 2021a.

Liang Xin, Wen Song, Zhiguang Cao, and Jie Zhang. Neurolkh: Combining deep learning model with lin-kernighan-helsgaun heuristic for solving the traveling salesman problem. In *Advances in Neural Information Processing Systems*, volume 34, pp. 7472–7483, 2021b.

Haoran Ye, Jiarui Wang, Zhiguang Cao, Helan Liang, and Yong Li. DeepACO: Neural-enhanced ant systems for combinatorial optimization. In *Advances in Neural Information Processing Systems*, 2023.

Haoran Ye, Jiarui Wang, Helan Liang, Zhiguang Cao, Yong Li, and Fanzhang Li. Glop: Learning global partition and local construction for solving large-scale routing problems in real-time. In *Proceedings of the AAAI Conference on Artificial Intelligence*, 2024.

Weihao Yu, Mi Luo, Pan Zhou, Chenyang Si, Yichen Zhou, Xinchao Wang, Jiashi Feng, and Shuicheng Yan. Metaformer is actually what you need for vision. In *Proceedings of the IEEE/CVF conference on computer vision and pattern recognition*, pp. 10819–10829, 2022.

Zhi Zheng, Changliang Zhou, Tong Xialiang, Mingxuan Yuan, and Zhenkun Wang. Udc: A unified neural divide-and-conquer framework for large-scale combinatorial optimization problems. In *Advances in Neural Information Processing Systems*, 2024.

Changliang Zhou, Xi Lin, Zhenkun Wang, Xialiang Tong, Mingxuan Yuan, and Qingfu Zhang. Instance-conditioned adaptation for large-scale generalization of neural combinatorial optimization. *arXiv preprint arXiv:2405.01906*, 2024a.

Jianan Zhou, Yaoxin Wu, Wen Song, Zhiguang Cao, and Jie Zhang. Towards omni-generalizable neural methods for vehicle routing problems. In *International Conference on Machine Learning*, pp. 42769–42789. PMLR, 2023.

Jianan Zhou, Zhiguang Cao, Yaoxin Wu, Wen Song, Yining Ma, Jie Zhang, and Chi Xu. Mvmoe: Multi-task vehicle routing solver with mixture-of-experts. In *International Conference on Machine Learning*, 2024b.

A   RELATED WORK

Neural VRP solvers typically learn construction heuristics, which can be broadly categorized into two types: autoregressive and non-autoregressive construction solvers. Autoregressive construction solvers build solutions sequentially by adding one feasible node at a time. Within this category, *light decoder-based solvers*, characterized by static node embeddings generated in a heavy encoder and solution construction handled by a lightweight decoder, have gained significant popularity for their computational efficiency and versatility. Vinyals et al. (2015) propose the Pointer Network, which solves the traveling salesman problem (TSP) using supervised learning (SL). Later works shift from SL to RL to solve TSP (Bello et al., 2017) and the capacitated vehicle routing problem (CVRP) (Nazari et al., 2018). Kool et al. (2019) introduce the attention model (AM), targeting a range of COPs such as TSP and CVRP. Building on this, Kwon et al. (2020) propose the policy optimization with multiple optima (POMO), which improves AM by exploiting a multi-trajectory strategy. Subsequent developments (Kwon et al., 2021; Kim et al., 2022; Grinsztajn et al., 2023; Liu et al., 2024; Gao et al., 2024; Hottung et al., 2024; Zhou et al., 2024b; Berto et al., 2024) are often built upon AM and POMO, further advancing their scalability (Li et al., 2021; Hou et al., 2023; Ye et al., 2024; Zheng et al., 2024) and generalization (Joshi et al., 2021; Bi et al., 2022; Geisler et al., 2022; Zhou et al., 2023). *Heavy decoder-based solvers* (Drakulic et al., 2023; Luo et al., 2023; 2024), characterized by dynamic node embeddings re-embedded at each decoding step, demonstrate impressive performance on large-scale instances, though at the expense of computational efficiency and training simplicity. Regarding non-autoregressive construction solvers, solutions are generated in a one-shot manner, bypassing the need for iterative forward passes through the model. Early work (Joshi et al., 2019) employs a graph convolutional network to predict the probability of each edge appearing on the optimal tour (i.e., a heatmap) using SL. More recent efforts (Fu et al., 2021; Qiu et al., 2022; Sun & Yang, 2023; Min et al., 2023; Ye et al., 2023; Kim et al., 2024; Xia et al., 2024) further enhance performance by leveraging advanced models, training paradigms, and search strategies. Beyond construction solvers, some neural solvers learn improvement heuristics to iteratively refine an initial feasible solution until a termination condition is met. These approaches often involve learning more efficient or effective search components within classical local search methods or specialized heuristic solvers (Chen & Tian, 2019; Lu et al., 2020; Costa et al., 2020; Wu et al., 2021; Ma et al., 2021; Xin et al., 2021b; Ma et al., 2023). While improvement solvers generally outperform construction solvers in terms of solution quality, they come with the trade-off of significantly longer inference time. In this paper, we mainly focus on autoregressive construction solvers due to their efficiency and versatility in solving VRPs.

B   MORE DISCUSSIONS ON LIGHT DECODER AND HEAVY DECODER

This paper bridges heavy decoder-based and light decoder-based methods through the concept of sharing encoding layers. This naturally leads to a more general paradigm: **for a model with L layers, the first L' layers are shared across K decoding steps**. Specifically, it becomes decoder-only (e.g., BQ (Drakulic et al., 2023)) when $L' = 0$, a heavy decoder (e.g., LEHD (Luo et al., 2023)) when $L' = 1$, and a light decoder (e.g., AM (Kool et al., 2019), POMO (Kwon et al., 2020)) when $L' = L - 1$. Such a framework offers flexible trade-offs between performance and efficiency by adjusting the number of shared layers and the frequency of updating shared embeddings. It may reduce the encoder's task complexity if static embedding is utilized for only a constant number of steps K (rather than all decoding steps). We leave a comprehensive investigation of this framework for future work.

C   IMPACT OF CAPACITY

We found that the POMON+IDT+FF model trained with fixed capacity data fail to generalize to scales that are very different from training setting even on small size data (see Table 6). This observation provides an insight: the **capacity setting might introduce generalization challenges independent of the problem scale**. This observation motivates us to explore varying capacity training to expose the model to a broader range of contexts.

Table 6: Investigation into the impact of capacity setting. POMON+IDT+FF trained from varying size Uniform(40, 100) capacity 50 data fail to generalize to varying capacity data. POMO no-aug single means the model is use single trajectory with no augmentation during inference, n100:Cap$M$ denotes data of size 100 sampled with capacity scalar M.

Method	n100:Cap50 Obj.	n100:Cap100 Obj.	n100:Cap250 Obj.	n100:Cap500 Obj.
POMON+IDT+FF no-aug single	16.20	11.14	9.04	8.65
LEHD greedy	16.55	11.17	8.81	8.41

D AVERAGE GAP IN CROSS-PROBLEM SETTINGS

Table 7: Average gap of each model in cross-problem settings.

Method	6 Trained VRPs	10 Unseen VRPs	ALL
POMO-MTL	2.863%	6.231%	4.968%
MVMoE-L	2.584%	5.989%	4.712%
MVMoE	2.515%	5.844%	4.596%
ReLD-MTL	2.054%	5.059%	3.932%
ReLD-MoEL	**1.974%**	**4.962%**	**3.842%**
ReLD-MoEL$^+$	2.172%	5.126%	4.019%

E RESULTS ON CVRPLIB SET-XXL

Table 8: Empirical results on real-world instances from CVRPLib Set-XXL with $N \leq 16,000$. The asterisk (*) denotes the results of methods directly obtained from the original paper.

	L1 (3K)	L2 (4K)	A1 (6K)	A2 (7K)	G1 (10K)	G2 (11K)	B1 (15K)	B2 (16K)
GLOP-LKH3*	16.60%	21.10%	19.30%	19.40%	18.30%	18.10%	27.50%	20.10%
BQ greedy*	13.27%	24.00%	11.21%	15.02%	-	-	-	-
LEHD greedy*	14.04%	26.30%	18.90%	26.40%	27.23%	38.45%	35.94%	40.76%
POMO*	75.30%	78.16%	112.27%	159.22%	-	-	-	-
Sym-POMO*	170.44%	179.55%	79.72%	179.55%	-	-	-	-
Omni-POMO*	22.79%	60.39%	42.52%	48.59%	-	-	-	-
ELG*	10.77%	21.80%	10.70%	17.69%	13.24%	18.93%	17.73%	20.05%
ReLD no-aug	7.74%	15.23%	7.61%	13.53%	7.92%	15.44%	10.45%	15.59%
ReLD	**7.45%**	**14.55%**	**7.43%**	**13.50%**	**7.63%**	**14.38%**	**10.08%**	**14.69%**

F APPLICATION ON ATSP

We further conduct preliminary experiments on the asymmetric travelling salesman problem (ATSP), which is a more practical and general TSP setting. The experiements are conducted on the MatNet model (Kwon et al., 2021).

F.1 ENCODER MODIFICATIONS

We make some simple adjustments to the original MatNet encoder to make it lighter and better, these modifications are applied to both the presented MatNet$^+$ baseline and ReLD.

Initial Embedding. Original MatNet use zero vectors and one-hot vectors for initial embeddings. However, using one-hot vectors limits the model's applicability to instances with size larger than embedding dimension (256). To resolve this, we assign a random number from Uniform(0, 1) to each node as its initial node features (need to cite goal). Then, a learnable linear layer transforms the 1D random features into the embedding dimension as inputs to the encoder.

Single Branch. MatNet adapt a two branch transformer architecture with cross-attention to model the interaction between two sets of objects. This design is redundent for ATSP, where there is only a single set of objects (i.e., nodes). Thus, we modify the encoder to include only a single branch with self-attention, reducing the number of parameters by nearly half.

Mixed Score Self-Attention. To modify the mixed score cross-attention proposed in MatNet to self-attention, we mix the distance matrix D and its transpose D^T simultaneously with the attention score of each head. This modification helps the network better understand the 'from-to' dual relationship between nodes with self-attention. Notably, we found that the model diverges in the single branch setting without D^T.

Normalized Distance Matrix. Since the optimal solution is invariant to the scale of the distance matrix, we normalize the distance matrix by dividing its maximum value before sending it to network.

F.2   ReLD for ATSP

We incoporate the proposed architectural design (i.e., identity mapping and feed-forward network) into the MatNet decoder. Specifically, let h_{τ_t} denote the embedding of the tth node of the constructed trajectory. At step $t + 1$, the query vector h'_c is obtained as follows:

$$h'_c = \text{MHA}([h_{\tau_t}, h_{\tau_1}], H_t, H_t) + h_{\tau_t},$$

where $[\cdot, \cdot]$ denotes the concatenation operator. Notice that we exclude the step-agnostic context information h_{τ_1} in the identity mapping. Then, we refine the obtained h'_c using a feed-forward network with reZero (Bachlechner et al., 2021):

$$q_c = \alpha h'_c + \text{FF}(h'_c),$$

where FF is a 2-layer feed-forward network with ReLU activation, α is a learnable scalar initialized to zero. The resulting q_c is then used in Eq. (5) of the paper to output probabilities for each node. Note that the distance heuristic and varying-size training are not utilized in this preliminary result.

F.3   Training Setting

We train the models on instances of size 100 for 2100 epochs, with each epoch contains 10000 instances and the batch size of 128. To reduce memory, we use 4 attention heads with qkv dimension equals to 64 in the encoder, other hyper-parameters remain the same as MatNet (Kwon et al., 2021).

F.4   Results

We test the models on synthetic data of sizes 20, 50, 100, 200, and 500. All the models use greedy rollout with full trajectories and without augmentation. For the original MatNet, we report the results from the released checkpoint, which is trained for 12,000 epochs on instances of size 100. MatNet$^+$ includes the modifications outlined in Section F.1 upon MatNet, while ReLD incorporates additional decoder changes upon MatNet$^+$. The results are presented in Table 9. It can be seen that the original MatNet model fails to generalize across sizes. MatNet$^+$ model significantly outperforms the original model, and ReLD achieves even better results across all sizes, with a more pronounced gap at larger sizes.

Table 9: Results on ATSP instances across different scales.

Method	ATSP20 Obj. (Gap)	ATSP50 Obj. (Gap)	ATSP100 Obj. (Gap)	ATSP200 Obj. (Gap)	ATSP500 Obj. (Gap)
CPLEX	1.540 (*)	1.560 (*)	1.570 (*)	-	-
MatNet official	2.608 (69.351%)	2.556 (63.846%)	1.624 (3.439%)	-	-
MatNet$^+$	1.651 (7.208%)	1.604 (2.821%)	1.616 (2.930%)	1.665 (1.216%)	2.126 (12.725%)
ReLD	1.623 (5.390%)	1.591 (1.987%)	1.607 (2.357%)	1.645 (*)	1.886 (*)

G   ABLATION STUDY RESULTS

The ablation results of the architectural components are presented in Table 10, the model ReLD w/o IDT&FF, ReLD-7Layer, and ReLD are trained under the setting described in Section 4.1, all other models are trained under the same condition as the POMO baseline. To better evaluate the effect of the distance heuristic on larger instances, we additionally trained ReLD with and without the distance heuristic under the training setting used in ICAM (Zhou et al., 2024a), which primarily trains on instances of size sampled from Uniform(100, 500). The results of this experiment is presented in Table 11.

Where and How to Introduce Extra Parameters Matter. We explore three additional ways to increase the number of parameters in the decoder: (1) +FF$_{qk}$: replacing the query and key transformtions in the MHA module with feed-forward networks, (2) +FF$_{qkv}$: replacing the query, key, and value transformtions in the MHA module with feed-forward networks, and (3) +MHA: adding an additional MHA layer on top of the original one. It can be observed that simply increasing the number of parameters does not consistently lead to better performance. In fact, certain modifications (+FF$_{qk}$ and +FF$_{qkv}$) degrade performance significantly, particularly on larger instances. This highlights the importance of thoughtfully determining where and how additional parameters are introduced into the decoder.

Why Identity Mapping is Effective for Size Generalization? The effectiveness likely stems from its ability to explicitly preserve context information, such as the location of the last selected node. As problem sizes grow, the decoder must aggregate a vast amount of global and local information into a fixed-size query vector, which can result in the loss of crucial locality information (Alon & Yahav, 2020). Identity mapping mitigates this issue by reinforcing the positional information of the last visited node, enabling the model to better distinguish local interactions in larger graphs.

Adding Additional Encoder Layers to ReLD Does Not Benefit Size Generalization. We also attempted to enhance the encoder capacity in ReLD by adding an additional layer (ReLD-7layer). Unfortunately, while this led to a slight improvement in in-distribution performance, it had no positive effect on OOD generalization, and in some cases, even worsened it. This supports the hypothesis that, with the same decoder structure, the encoder's learning task for small-scale instances has limited overlap with that for larger-scale problems, as indicated by the intrinsic complexity gap. As a result, improving the encoder alone does not necessarily enhance OOD performance due to this misalignment. These findings suggest that efforts should focus on improving the decoder structure to simplify the encoder's task and reduce the gap between the encoder's tasks across different scales.

Distance Heuristic is Crucial. It can be observed that the distance heuristic plays a crucial role in enabling generalization across scales. When distance information is explicitly leveraged, models consistently achieve better performance across all problem sizes. For instance, ReLD with distance heuristic outperforms its counterpart without distance heuristic in all configurations, particularly on larger-scale instances such as CVRP5000 and CVRP7000. Notably, even without leveraging distance information, ReLD remains highly competitive with the baselines, particularly as problem sizes increase. This highlights the superiority of the proposed decoder modifications.

H   RESULTS OF FINE-TUNING ON LARGE SCALE INSTANCES

We fine-tune the ReLD model checkpoint from the 70th epoch (before to the learning rate decay) for 1 epoch (5,000 batches). The instance are generarated with size N sampled from Uniform(100, 500). The expected route size (average number of nodes in a route) is sampled from triangular distribution $T(8, 16, 45)$. The learning rate is decayed by a factor of 0.1 at the 2500th batch. Batch size is set to $[120 \cdot (\frac{100}{N})^{1.6}]$, around 150,000 instances are utilized in total for fine-tuning. Other settings remain identical to the training settings. For baseline, we train ELG under the same fine-tuning setting. the results are presented in Table 12. It can be seen that ReLD also achieves better fine-tuning performance in both in-distribution data (100, 200, and 500) and out-of-distribution data (1000).

Table 10: Ablation study of components in ReLD.

Method	CVRP100 Gap	CVRP200 Gap	CVRP500 Gap	CVRP1000 Gap
POMO	1.004%	3.403%	11.135%	110.632%
POMO+IDT	0.936%	3.096%	9.349%	23.508%
POMON	0.947%	3.864%	13.008%	33.262%
POMON+FF$_{qk}$	0.889%	3.907%	15.589%	169.461%
POMON+FF$_{qkv}$	0.837%	3.894%	16.314%	245.524%
POMON+MHA	1.129%	4.478%	15.809%	47.132%
POMON+IDT	0.909%	3.623%	10.932%	20.687%
POMON+FF	**0.663%**	3.142%	12.901%	35.589%
POMON+IDT+FF	0.682%	2.640%	8.185%	18.076%
ReLD w/o IDT&FF	1.063%	1.960%	4.101%	9.623%
ReLD-7Layer	0.921%	**1.638%**	3.055%	6.834%
ReLD	0.960%	1.690%	**3.015%**	**6.771%**

Table 11: Effects of training on larger-scale instances. 'w. dist' indicates that distance information is explicitly incorporated into the model, while 'w/o dist' denotes the absence of such information. 'Single-trajec.' refers to inference using a single starting point, '100-traject.' involves rolling out the top 100 starting points at the first step, and 'full-traject.' utilizes the total number of possible trajectories as in POMO. Augmentation is disabled for all models.

Method	CVRP100 Obj.	CVRP1000 Obj.	CVRP2000 Obj.	CVRP5000 Obj.	CVRP7000 Obj.
HGS	15.56	36.29	57.20	126.20	172.10
GLOP-G	**15.65**	**37.09**	63.02	140.35	191.20
LEHD greedy	16.22	38.91	61.58	138.17	-
BQ greedy	16.07	39.28	62.59	139.84	-
ICAM w. dist single-trajec.	16.19	38.97	62.38	140.25	-
ICAM w. dist full-trajec.	15.94	38.42	61.34	136.93	-
ReLD w/o dist single-trajec.	16.28	38.83	61.37	135.30	183.79
ReLD w/o dist 100-trajec.	15.98	38.41	60.78	134.45	182.75
ReLD w. dist single-trajec.	16.26	38.69	60.41	129.66	173.91
ReLD w. dist 100-trajec.	15.97	38.28	**59.84**	**128.79**	**172.83**

Table 12: Effects of fine-tuning on instances from Uniform(100, 500).

Method	CVRP100 Gap	CVRP200 Gap	CVRP500 Gap	CVRP1000 Gap
ELG	1.156%	4.150%	8.527%	15.054%
ELG fine-tune	1.895%	1.841%	2.281%	5.631%
ReLD	1.143%	2.036%	3.623%	7.156%
ReLD fine-tune	1.148%	1.675%	1.952%	3.947%

I ReLD Benefits from More Decoder Layer

To explore the potential gains of further increasing decoder capacity, we introduce ReLD-Large, which stacks an additional decoder block on top of the original ReLD decoder while preserving the property of static keys and values.

In specific, the original ReLD decoder can be viewed as a transformer block with a single query. We stack another single query block on top of the original one to further transform the query vector q_c obtained from Eq. (9): $z_c = \text{MHA}(q_c, H_t, H_t) + q_c$, $q'_c = z_c + \text{FF}(z_c)$. The transformed q'_c will

be used as input to the compatibility layer. To minimize the additional memory cost, the new block shares the same cached keys and values used in Eq. (11) (i.e., share the W^K, W^V parameters with the MHA module in Eq. (11). To maintain the total number of transformer blocks consistent with the original ReLD, we reduce the number of encoder blocks in ReLD-Large to 5.

The results are presented in Table 13. Both models use 100-trajectories with instance augx8 during inference. Notably, these experiments are conducted on different hardware than specified in the paper, resulting in ReLD's runtime differing from the values reported in Table 3. It can be observed that increasing the decoder's complexity further enhances model performance across all sizes, albeit with greater computational overhead.

Table 13: Results of stacking an additional layer in the decoder.

Method	CVRP100 Gap (time)	CVRP200 Gap (time)	CVRP500 Gap (time)	CVRP1000 Gap (time)
ReLD	0.959% (2.16m)	1.654% (0.11m)	2.975% (0.48m)	6.757% (1.95m)
ReLD-Large	0.891% (3.60m)	1.527% (0.16m)	2.678% (0.73m)	6.265% (2.89m)